Comput Mech (2007) 41:121–133
DOI 10.1007/s00466-007-0173-y

ORIGINAL PAPER

Finite cell method

h- and *p*-extension for embedded domain problems in solid mechanics

Jamshid Parvizian · Alexander Düster · Ernst Rank

Received: 21 August 2006 / Accepted: 8 March 2007 / Published online: 3 April 2007

Abstract A simple yet effective modification to the standard finite element method is presented in this paper. The basic idea is an extension of a partial differential equation beyond the physical domain of computation up to the boundaries of an embedding domain, which can easier be meshed. If this extension is smooth, the extended solution can be well approximated by high order polynomials. This way, the finite element mesh can be replaced by structured or unstructured cells embedding the domain where classical *h*- or *p*-*Ansatz* functions are defined. An adequate scheme for numerical integration has to be used to differentiate between inside and outside the physical domain, very similar to strategies used in the *level set* method. In contrast to earlier works, e.g., the extended or the generalized finite element method, no special interpolation function is introduced for enrichment purposes. Nevertheless, when using *p*-extension, the method shows exponential rate of convergence for smooth problems and good accuracy even in the presence of singularities. The formulation in this paper is applied to linear elasticity problems and examined for 2D cases, although the concepts are generally valid.

Keywords Finite cells · Embedded domain · *p*-extension · Meshless methods

The first author would like to appreciate the financial support of his stay in Germany, where this research has been carried out, by the *Alexander von Humboldt* foundation.

J. Parvizian (✉)
Isfahan University of Technology, Isfahan, 84156 83111, Iran
e-mail: japa@cc.iut.ac.ir

J. Parvizian · A. Düster · E. Rank
Technische Universität München,
Lehrstuhl für Bauinformatik, München, Germany
e-mail: japa@inf.bv.tum.de

A. Düster
e-mail: duester@bv.tum.de

E. Rank
e-mail: rank@bv.tum.de

1 Introduction

Since the invention of the finite element method in 1950s numerous researches have been carried out to justify the mathematical foundations of the method, to develop techniques in order to increase the accuracy of the results or to decrease the cost of computations, and to make the application of the method as user-friendly as possible. However, for mesh generation as one key step in using the method even today not all major questions are fully answered. Problems arise when pure hexahedral meshes are desired, when structures are defined only implicitly by measurements like X-ray tomography, when the domain of computation is strongly distorted like in metal forming, when the material is ripped away or torn apart through processes like explosion or impact, or when free and moving boundary problems are considered.

Many attempts have been made over the past decades to relieve from the necessity of an exact meshing of the domain of computation. A vast literature is available, where very often different denotations are used for similar techniques. An early suggestion to embed the (a priori unknown) domain of computation into a larger computational mesh was suggested in [16] for a seepage flow problem, based on an adaptive *h*-version finite element method. The flow regime was only defined implicitly by imposing appropriate

integration techniques and transforming the free boundary problem formally into a formulation with nonlinear material properties. Instead of a sharp boundary of the seepage regime a smooth transition from the flow to the non-flow domain was used, very similar to the recently suggested *fat boundary method* [10] of Ismail. This technique, being related to approaches which are well-known today as *level set methods* (see, e.g. [12,20]), was extended in the late 1980s to industrial applications for the simulation of moving boundary problems in semiconductor process simulation [13,17,18].

In the 1990s, a wide variety of papers on meshless methods appeared with the objective to construct approximations entirely in terms of nodes but not node connectivities [3]. Major, and up to now only partially solved, problems are optimal distribution patterns of the nodes, possible discontinuities of parameters within the domain of computation, and proper and efficient implementation of boundary conditions.

Parallel to efforts to develop meshless methods, extension of the domain of computation as well as of the approximation spaces was considered by Duarte et al. [5] and also by Strouboulis et al. [22]. The essential aspect of similar versions of the extension, such as *eXtended Finite Element Method* (XFEM) or *Generalized Finite Element Method* (GFEM) reported so far, is the enrichment of the approximation, using a partition of unity method, by the a priori knowledge of the solution in special cases, such as singular corners. These methods rely on so called *library functions* and adaptive integration schemes.

Another line of research has been directed toward embedding the domain while the field variables go continuously beyond the physical boundary, [2,4,11,19]. Application of these methods has been mainly confined to optimal design problems, and low order elements were used in all cases. Similar techniques used in domain embedding methods are developed under different versions of *fictitious domain methods*. The core idea is again to immerse the original domain into a geometrically bigger and simpler one [15]. Finite difference, finite volume and low order finite element methods have been used to discretize the fictitious domain, see for example [4,14,21,25]. To treat the boundary conditions, the literature provides a wide scope of ideas and techniques similar in nature but different in names, such as *Lagrange multiplier method* [9] or *fat boundary method* [10].

In the present work, to discretize the domain of computation and the embedding domain, a finite number of computational *cells* is used, which cover the domain and may have simple shapes like squares or cubes. The field variable, e.g. the displacement, is *smoothly* extended beyond the cells cut by the original boundary. Numerically, the fictitious material is set extremely soft outside the physical domain, thus guaranteeing that the strain energy of the solutions in the original and the extended domains remains the same. Special integration techniques are employed to treat cells cut by the boundary. Stiffness matrices for all other cells are computed using classic FE techniques. This idea of using a "soft" material in void regions of a domain has been frequently used in the optimization literature, see for example [1].

Using high order Ansatz functions to approximate the extended variables is the most important aspect of the current work, not mentioned before in the relevant literature to the best of the authors' knowledge. A mathematical proof is sketched, and numerical studies are presented showing that the method yields *exponential rate of convergence* for smooth problems until the integration error dominates the discretization error. The error of the method is investigated in the energy norm and also pointwise, showing that, even for "porous" domains with many inclusions, very accurate solutions can be obtained. The numerical convergence study for solid mechanics problems is also extended to non-smooth problems with a detailed look into possibilities of improving accuracy in the neighborhood of singularities.

2 Finite cell method

2.1 Basic formulation

The finite cell method is an extension to the classical finite element method. Therefore, the main concepts and notations of finite elements are used. Without losing generality, this paper concentrates on 2D linear elasticity problems.

Let us assume that on a domain Ω with the boundary $\partial\Omega$ a problem of linear elasticity is described in weak form by

$$\mathcal{B}(\mathbf{u}, \mathbf{v}) = \mathcal{F}(\mathbf{v}) \tag{1}$$

where the bilinear form is

$$\mathcal{B}(\mathbf{u}, \mathbf{v}) = \int_{\Omega} [\mathbf{L}\,\mathbf{v}]^{\mathrm{T}}\,\mathbf{C}\,[\mathbf{L}\,\mathbf{u}]\,\mathrm{d}\Omega \tag{2}$$

in which $\mathbf{u}$ is the displacement, $\mathbf{v}$ is the test function, $\mathbf{L}$ is the standard strain–displacement operator and $\mathbf{C}$ is the elasticity matrix. Without loss of generality we assume homogeneous Dirichlet boundary conditions along Γ_D and a Neumann boundary Γ_N with prescribed tractions, $\partial\Omega = \Gamma_D \bigcup \Gamma_N$, and $\Gamma_D \bigcap \Gamma_N = \emptyset$.

The linear functional

$$\mathcal{F}(\mathbf{v}) = \int_{\Omega} \mathbf{v}^{\mathrm{T}}\mathbf{f}\,\mathrm{d}\Omega + \int_{\Gamma_N} \mathbf{v}^{\mathrm{T}}\mathbf{t}_N\,\mathrm{d}\Gamma \tag{3}$$

considers the volume loads $\mathbf{f}$ and prescribed tractions $\mathbf{t}_N$.

The domain of computation Ω is now embedded in the domain Ω_e with the boundary $\partial\Omega_e$, Fig. 1. The interface

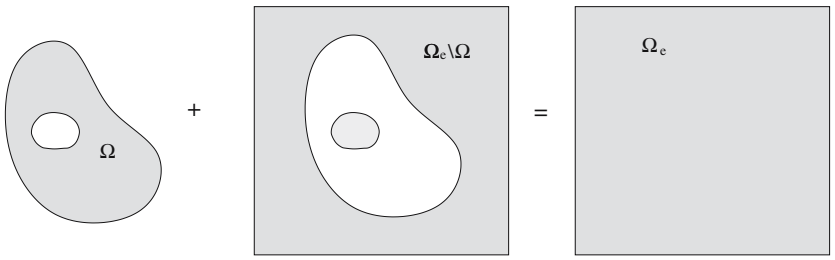

Fig. 1 The domain Ω is extended to Ω_e

between Ω and the extension is defined as $\Gamma_I = \partial\Omega \backslash (\partial\Omega \bigcap \partial\Omega_e)$, and it is first assumed that the Dirichlet boundary Γ_D of Ω does not intersect Γ_I. This is, e.g. the case for structures where the extended domain covers stress free voids in the interior of Ω. The more general case of extension across Dirichlet boundary conditions is discussed in Sect. 2.2.

Following [11], the displacement variable, $\mathbf{u}$ is defined as:

$$\mathbf{u} = \begin{cases} \mathbf{u}^1 & \text{in } \Omega \\ \mathbf{u}^2 & \text{in } \Omega_e \setminus \Omega \end{cases} \tag{4}$$

while the transition conditions guarantee the continuity at the interface between Ω and $\Omega_e \setminus \Omega$:

$$\begin{aligned} \mathbf{t}^1 &= \mathbf{t}^2 \quad \text{on } \Gamma_I \\ \mathbf{u}^1 &= \mathbf{u}^2 \quad \text{on } \Gamma_I \end{aligned} \tag{5}$$

Boundary conditions are set for Ω_e:

$$\begin{aligned} \bar{\mathbf{t}} &= \mathbf{0} \quad \text{on } \Gamma_1 \\ \bar{\mathbf{u}} &= \mathbf{0} \quad \text{on } \Gamma_2 \end{aligned} \tag{6}$$

in which $\bar{\mathbf{t}}$ and $\bar{\mathbf{u}}$ are the specified tractions and displacements on the Neumann, (Γ_1), and Dirichlet, (Γ_2), boundaries respectively, $\partial\Omega_e = \Gamma_1 \bigcup \Gamma_2$, and $\Gamma_1 \bigcap \Gamma_2 = \emptyset$. The second condition in (6) is in general necessary to avoid rigid body motion.

The weak form of the equilibrium equation for the embedding domain Ω_e is given as

$$\mathcal{B}_e(\mathbf{u}, \mathbf{v}) = \mathcal{F}_e(\mathbf{v}) \tag{7}$$

where the bilinear form is

$$\mathcal{B}_e(\mathbf{u}, \mathbf{v}) = \int_{\Omega_e} [\mathbf{L}\,\mathbf{v}]^{\mathrm{T}}\, \mathbf{C}_e\, [\mathbf{L}\,\mathbf{u}]\, \mathrm{d}\Omega \tag{8}$$

in which $\mathbf{C}_e$ is the elasticity matrix of the extended domain, given as

$$\mathbf{C}_e = \begin{cases} \mathbf{C} & \text{in } \Omega \\ \mathbf{C}^* & \text{in } \Omega_e \setminus \Omega \end{cases} \tag{9}$$

Note that in the case of a "zero extension", where $\mathbf{C}^* = \mathbf{0}$, the bilinear functional (8) turns to

$$\begin{aligned} \mathcal{B}_e(\mathbf{u}, \mathbf{v}) &= \int_{\Omega} [\mathbf{L}\,\mathbf{v}]^{\mathrm{T}}\, \mathbf{C}\, [\mathbf{L}\,\mathbf{u}]\, \mathrm{d}\Omega + \int_{\Omega_e \setminus \Omega} [\mathbf{L}\,\mathbf{v}]^{\mathrm{T}}\, \mathbf{0}\, [\mathbf{L}\,\mathbf{u}]\, \mathrm{d}\Omega \\ &= \int_{\Omega_e} [\mathbf{L}\,\mathbf{v}]^{\mathrm{T}}\, \alpha\mathbf{C}\, [\mathbf{L}\,\mathbf{u}]\, \mathrm{d}\Omega = \mathcal{B}(\mathbf{u}, \mathbf{v}) \end{aligned} \tag{10}$$

in which

$$\alpha = \begin{cases} 1.0 & \text{in } \Omega \\ 0.0 & \text{in } \Omega_e \setminus \Omega \end{cases} \tag{11}$$

The linear functional

$$\mathcal{F}_e(\mathbf{v}) = \int_{\Omega_e} \mathbf{v}^{\mathrm{T}}\mathbf{f}\, \mathrm{d}\Omega + \int_{\Gamma_N} \mathbf{v}^{\mathrm{T}}\mathbf{t}_N\, \mathrm{d}\Gamma + \int_{\Gamma_1} \mathbf{v}^{\mathrm{T}}\bar{\mathbf{t}}\, \mathrm{d}\Gamma \tag{12}$$

considers the volume loads $\mathbf{f}$, prescribed traction $\mathbf{t}_N$ along Γ_N *interior* to Ω_e and prescribed traction $\bar{\mathbf{t}}$ at the boundary of the extended domain. Due to the first condition in (6), the last term in (12) can be assumed 0.

The extended domain is now discretized in a mesh being independent of the original domain. These "finite elements" of the extended domain do not necessarily fulfill the usual geometric properties of elements for the original domain Ω, as they may be intersected by $\partial\Omega$. To distinguish from classical elements they will be called *finite cells*. For simplicity, we will first assume cells to be squares (see Fig. 2), but in the numerical examples applications with general quadrilaterals cells also will be reported.

The union of all cells forms the extended domain

$$\Omega_e = \bigcup_{c=1}^{m} \Omega_c \tag{13}$$

where Ω_c is the domain represented by a cell, and the extended domain is divided into m cells.

At the discretized level, (8) turns to:

$$\mathcal{B}_e(\mathbf{u}, \mathbf{v}) = \sum_{c=1}^{m} \int_{\Omega_c} [\mathbf{L}\,\mathbf{v}]^{\mathrm{T}}\, \mathbf{C}_e\, [\mathbf{L}\,\mathbf{u}]\, \mathrm{d}\Omega \tag{14}$$

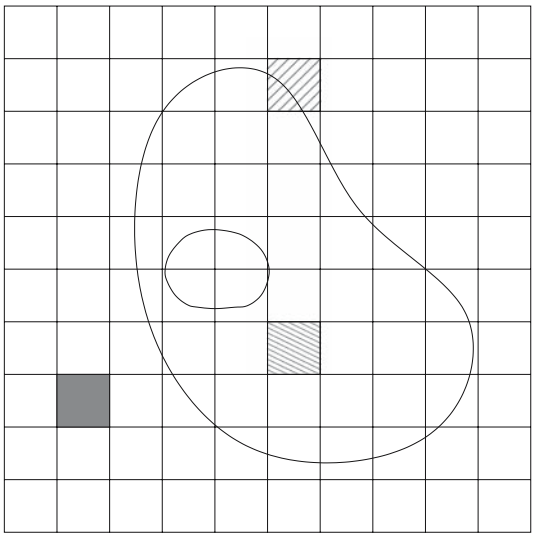

Fig. 2 The extended domain Ω_e is discretized using simple quadrilateral cells

In each cell, the displacement variable is approximated as

$$\mathbf{u} = \mathbf{NU} \tag{15}$$

in which $\mathbf{N}$ denotes the matrix of appropriate shape functions and $\mathbf{U}$ is the vector of unknowns. In our implementation [6] hierarchical shape functions based on (integrated) Legendre polynomial (see, e.g. [23,24]) are used, allowing h-extension for low as well as higher polynomial orders by refinement of the cells and also a p-extension on a fixed mesh of (coarse) cells.

Based on the Bubnov-Galerkin approach, $\mathbf{v} = \mathbf{NV}$, inserting (15) into (14) results in the finite cell formulation as

$$\mathbf{KU} = \mathbf{F} \tag{16}$$

where $\mathbf{K}$, the global stiffness matrix, is the result of proper assembling of $\mathbf{k}^c$, given as

$$\mathbf{k}^c = \int_{-1}^{+1}\int_{-1}^{+1} (\mathbf{LN})^{\mathrm{T}}\mathbf{C_e}(\mathbf{LN}) \parallel \mathbf{J} \parallel \mathrm{d}\xi\, \mathrm{d}\eta \tag{17}$$

in which $\parallel \mathbf{J} \parallel$ is the determinant of the Jacobian matrix of mapping:

$$\mathbf{J} = \begin{pmatrix} \dfrac{\partial x(\xi,\eta)}{\partial \xi} & \dfrac{\partial y(\xi,\eta)}{\partial \xi} \\ \dfrac{\partial x(\xi,\eta)}{\partial \eta} & \dfrac{\partial y(\xi,\eta)}{\partial \eta} \end{pmatrix} \tag{18}$$

2.2 Boundary conditions

To apply boundary conditions, when cell boundaries and the boundary $\partial\Omega$ do not conform, several approaches, such as "Distributed Lagrangian", the "Fat Boundary", "Elimination" and "Penalty" Methods (see, e.g. [4,11]) could be used. Common in all of these approaches is the idea of minimizing the energy functional subject to equality conditions.

Let us first consider homogeneous Neumann conditions from a mechanical point of view. This "zero traction condition" is equivalent to assuming material with zero stiffness in the extended domain, e.g. setting $\mathbf{C}^* = \mathbf{0}$. Inhomogeneous Neumann condition can be realized by explicitly including the first line integral in (12), i.e. by integrating over Γ_N as a curve interior to Ω_e.

Homogeneous Dirichlet conditions can be approximated by assuming a "stiff strip" of material from Γ_D up to the Dirichlet boundary Γ_2 of the extended domain. Our numerical experiments show that $\alpha = \mathcal{O}(10)$, i.e. the assumption of a material being one order of magnitude stiffer than in the original domain of computation gives reasonably accurate results. We believe that assuming a stiff support is well in agreement with the physical model, for the support is never absolutely rigid in real world.

2.3 Numerical integration

The approximation of the original problem (2) over the domain Ω has been replaced by a problem over an extended domain, yet with discontinuous coefficients. Therefore the integrand in (14) may be discontinuous within cells being cut by the boundary $\partial\Omega$. An adapted integration scheme is necessary to capture this discontinuity.

Different variants have been investigated. Low order integration like trapezoidal rule on a refined grid of sub-cells can be used (Fig. 3) while the integration points are distributed

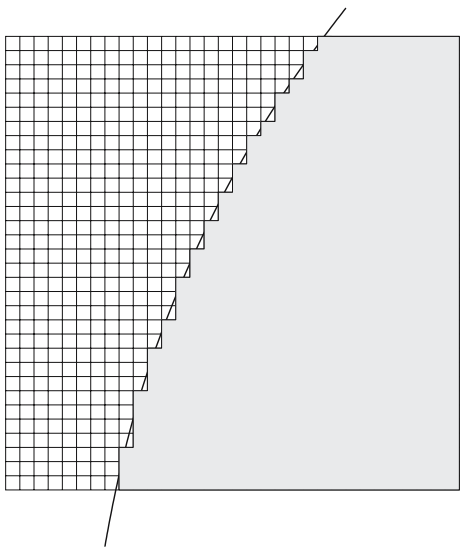

Fig. 3 When a cell is cut by the boundary, the integration scheme considers only the part interior to Ω

uniformly in the cell. Also Gaussian integration with higher number of integration points on the original cell or on sub-cells is applicable. This approach is used in some of the examples presented later in this paper. Another alternative is to use a quadtree technique subdividing the cut cell to non-uniform smaller cells for adaptive integration. The question of the most efficient integration scheme for cut cells is however still open.

To avoid ill conditioning of the global stiffness matrix, cells completely outside Ω can be ignored for integration and assembly, or a small non-zero α can be used for such cells. Our numerical experiences show that any α as small as 10^{-10} can replace zero. The domain integral in the linear functional (12) can be dealt with in the extended domain by introducing α and using the same procedure as for the bilinear form.

2.4 Convergence properties

For simplicity, we will only consider the case of a traction free boundary on Γ_I. Typical examples fulfilling this condition are structures, where interior voids are covered by the extended domain (for instance, see examples in the next section). In this case, is $\mathbf{C}^* = \mathbf{0}$ in (9).

By construction, the finite cell approximation $\mathbf{u}_{\mathrm{FC}}$ on Ω to the exact solution $\mathbf{u}_{\mathrm{ex}}$ of (1) is a restriction of the finite element approximation $\mathbf{u}_{\mathrm{FE}}$ on the extended domain Ω_e to $\mathbf{u}_{e,\mathrm{ex}}$ of (7). Therefore, convergence properties of the finite cell method can be derived from those of the associated finite element computation. The following first remarks can be made:

- $\mathbf{u}_{e,\mathrm{ex}}$ is not determined uniquely in $\Omega_e \setminus \Omega$, as, due to $\mathbf{C}^* = \mathbf{0}$, no energy is contributed to the bilinear form (7). Yet, the energy norm of $\mathbf{u}_{e,\mathrm{ex}}$ is uniquely determined.
- The restrictions on each exact extended solution to Ω and the solution to (1) are identical:

$$\mathbf{u}_{\mathrm{ex}} = \mathbf{u}_{e,\mathrm{ex}} \quad \text{in } \Omega \tag{19}$$

- Although *data* are non-smooth in Ω_e, there are extended solutions $\mathbf{u}_{e,\mathrm{ex}}$ which are smooth up to points in Ω, where $\mathbf{u}_{\mathrm{ex}}$ has singularities.
- By nature of the method, the "best approximation" argument for Galerkin's method holds in Ω_e and can therefore be transferred to the finite cell method:

$$\begin{aligned} \| \mathbf{u}_{\mathrm{FC}} - \mathbf{u}_{\mathrm{ex}} \|_{\Omega} &= \| \mathbf{u}_{\mathrm{FC}} - \mathbf{u}_{e,\mathrm{ex}} \|_{\Omega} \\ &= \| \mathbf{u}_{\mathrm{FE}} - \mathbf{u}_{e,\mathrm{ex}} \|_{\Omega_e} \\ &\leq \| \mathbf{w} - \mathbf{u}_{e,\mathrm{ex}} \|_{\Omega} \end{aligned} \tag{20}$$

for any $\mathbf{w}$ in the finite element space of the extended domain.

Using these observations, we can distinguish between the following cases:

- *Case 1*: There is an analytic extension of $\mathbf{u}_{\mathrm{ex}}$ to Ω_e. Obviously this is true if and only if $\mathbf{u}_{\mathrm{ex}}$ is analytic itself, i.e. if the original problem has smooth solution up to the boundary $\partial\Omega$.
  - *h-extension*: The convergence rate of the FCM is the same as that of FEM on the extended domain, i.e. algebraic and identical to a finite element h-extension on Ω, (see Example 3.1.1).
  - *p-extension*: As $\mathbf{u}_{e,\mathrm{ex}}$ is smooth, convergence is exponential on Ω_e and therefore also on Ω, (see Examples 3.1.2 and 3.2).
- *Case 2*: $\mathbf{u}_{\mathrm{ex}}$ has singular points at the boundary of Ω which are located at nodes of the finite cells. $\mathbf{u}_{\mathrm{ex}}$ can be extended to Ω_e, yet only with singularities in the interior of the extended domain. The finite element approximation is affected by singularities at nodes of its elements. Convergence rate is algebraic for h- and p-extension and equal to that of a classical finite element approximation on Ω. p-extension will converge at twice the rate of h-extension (see [23,24]) and a preasymtotic exponential rate of convergence may be observed, (see Example 3.3.2).
- *Case 3*: $\mathbf{u}_{\mathrm{ex}}$ has singular points at the boundary of Ω which are *not* located at nodes of the finite cells. Now, $\mathbf{u}_{\mathrm{FE}}$ must approximate a solution with singularities in the *interior* of elements. For h- and p-extension convergence rate is algebraic and lower than in Case 2, (see Example 3.3.1). Yet, the FCM-solution can be significantly improved by a strictly local modification of the cell pattern, (see Example 3.3.4).

3 Numerical examples

In this section numerical examples are provided to demonstrate the performance of the method for regular problems and for problems with singularities. In all examples, plane-stress problems of linear elasticity are considered and the material used is steel with Young modulus and Poisson ratio respectively as $E = 206.9\,\mathrm{GPa}$, and $\nu = 0.29$. Reference solutions are obtained by a p-version finite element extension using either a fine or a well-manipulated geometric coarse mesh while the polynomial degree p of the approximation is increased until the strain energy changes remain within a very small tolerance.

Examples presented here are solved using AdhoC, which is an h- and p-version FE code developed at the Technische Universität München [6] modified for the finite cell

formulation. GiD [8] is used for post-processing aims. A fine post processing mesh is used, if necessary.

3.1 Perforated plate

3.1.1 h-extension for smooth problems

In the first example, symmetry conditions are applied on the left and lower boundaries (see Fig. 4), and traction free boundary conditions are assumed at the void. The reference solution is achieved by a finite element p-extension on a mesh of four elements which describe the exact geometry using the blending function method [23,24]. The interpolation degree, p, is increased from 1 to 20 yielding an estimate for the strain energy as 0.7021812127.

Different strategies are used to inspect the FCM. First of all, h-extension convergence in energy norm is checked by refining from a coarse cell distribution, while $p = 1$. The number of cells in each direction is chosen as odd so that any chance of cells matching the boundary points of the circular hole is omitted. A simple integration scheme with a high Gaussian order, e.g. 20 or more, is used. The convergence rate is then compared with a reference h-finite-element extension, using a quasi-uniform, yet unstructured, boundary matching mesh. Table 1 gives the convergence data.

As shown in Fig. 5 the rate of convergence and even the convergence constants (e.g. the offset of the convergence curves) are nearly the same for FCM and FEM. When subtracting all degrees of freedom of cells being completely inside the void (which need not be assembled to the global equation system and therefore add no significant cost to the computation) the convergence curve of FCM would even be shifted down by 20%. On the other hand, the convergence constant of the FEM-h-extension may be improved by rearranging the elements to minimize the discretization error from distortion of elements. One may conclude however, that the error introduced by integrating over cells covering both material and void does not dominate the discretization error of the h-extension process. In Fig. 5, the slope of the lines for both solutions is 0.5, as expected.

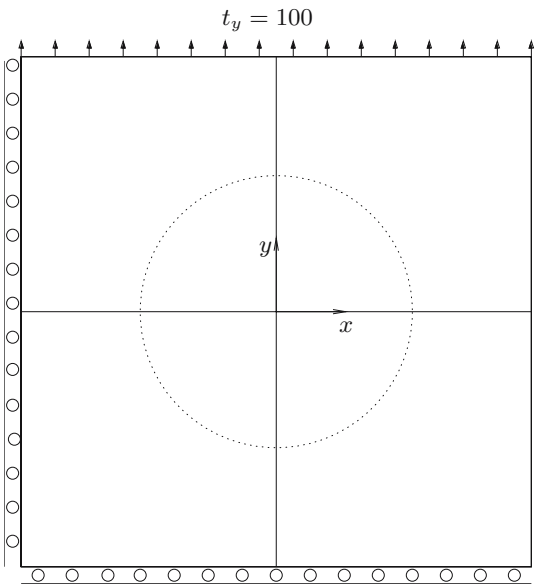

Fig. 4 The perforated square plate (4.0×4.0) under symmetric boundary conditions. The plate is divided to 2×2 cells

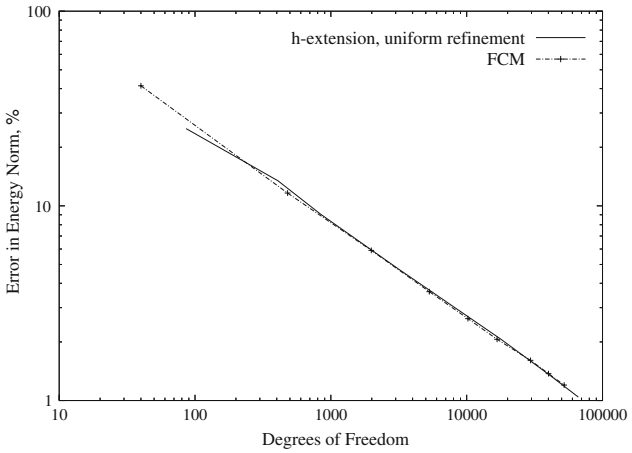

Fig. 5 Convergence of the strain energy for h-refinement of FEM and FCM, *p=1*

Table 1 Perforated plate. Convergence of the strain energy for h-refinement of FEM and FCM, $p = 1$

Finite elements	DOF	Strain energy	Finite cells	DOF	Strain energy
32	86	0.6585574280	4×4	40	0.5819857730
179	408	0.6894846484	15×15	480	0.6926786278
386	842	0.6964228007	31×31	1984	0.6997327267
1511	3164	0.7006122930	51×51	5304	0.7012578429
5618	11522	0.7017252739	71×71	10224	0.7016942625
8709	17776	0.7018800900	91×91	16744	0.7018824489
14957	30388	0.7020076127	121×121	29524	0.7019994708
20893	42352	0.7020582064	141×141	40044	0.7020484429
32844	66398	0.7021050534	161×161	52164	0.7020801016

3.1.2 p-extension for smooth problems

To investigate p-extension, the perforated plate is now discretized into 2×2 cells, only. To be able to decrease the error due to integration, each cell cut by the boundary is subdivided to 6×6 square sub-cells first. Gaussian integration with 50 integration points in each direction in the cut sub-cells is used. In another attempt, only 2×2 sub-cells and Gaussian integration scheme with extremely high number of integration points, 96, is chosen. Figure 6 shows the convergence of the algorithm versus the DOF while the polynomial degree, p, is increased. In both cases FCM converges exponentially like a reference p-FEM-approximation until the integration error starts to dominate and the convergence curves level off. Using 6×6 sub-cells, the integration error is negligible, an exponential convergence is achievable at least up to $p = 10$ where the error in energy norm is about 0.2%. This figure suggests that a proper integration scheme can enormously improve the results. Similar rate of convergence is observed if more cells are used.

It is worth mentioning that the displacement field in the FCM is extended continuously beyond the physical domain. This is well demonstrated in Fig. 7 and supports the argument given in Sect. 2.4 on the convergence properties of the method.

Although the energy norm is a good global error measure, point-wise values of stresses are similarly important for engineering applications. To see how these stresses are comparable to the reference solution, let us consider two cut-lines, one diagonal from $(-2, -2)$ to $(2, 2)$, the other horizontal, from $(-2, 0)$ to $(2, 0)$, which is critical since it passes the stress concentrated region. The domain is discretized into 15×15 cells, no sub-cells are used for integration while the Gaussian order is 50 in the cut cells, and the polynomial degree is taken as $p = 3$. As shown in Fig. 8, the von Mises stress distribution along each cut-line nearly perfectly matches the reference solution. The maximum error of the von Mises stress is about 1%.

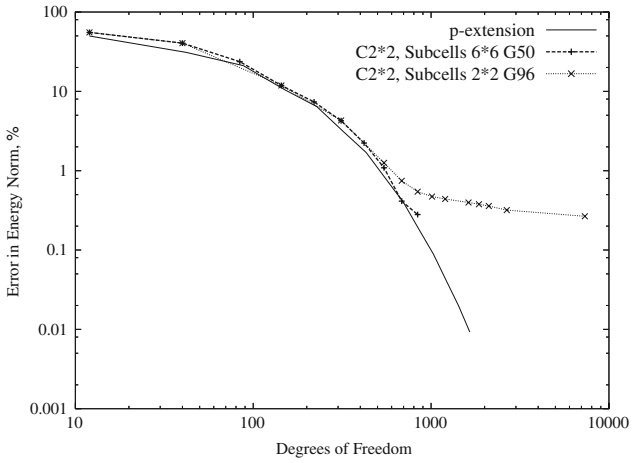

Fig. 6 A comparison between the FCM- and FEM-p-extension. 2×2 quadrilateral cells are used for the perforated square

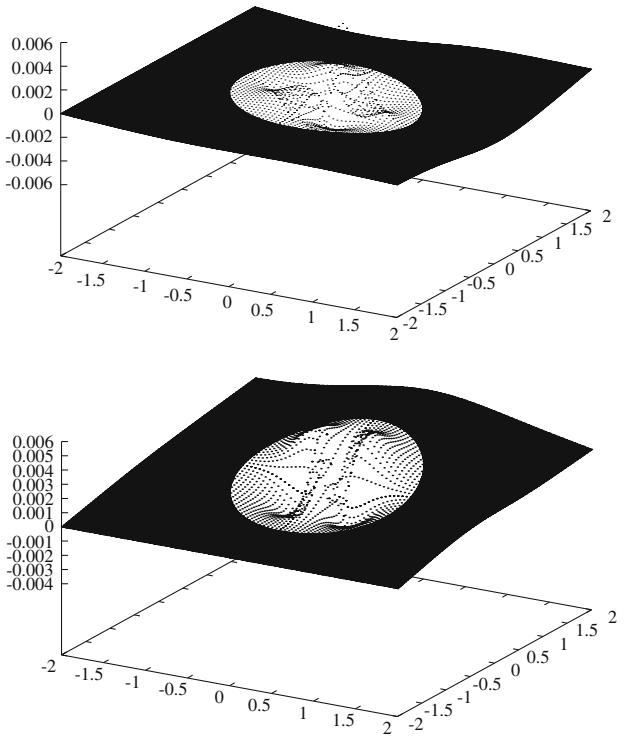

Fig. 7 The displacement in x- (*top*) and y- (*bottom*) directions are given for both FE and FCM solutions. As shown, the field is continuously extended

Figure 9 presents the von Mises stress contours throughout the perforated plate using FCM, 2×2 cells and $p = 10$, with the reference solution. As shown, the method has been able to capture the highly varying stresses even in the regions cut by the boundary.

As implementation issues play an essential role, it is difficult to compare the computational effort for different numerical methods. Nevertheless, we briefly want to discuss the CPU time for the finite cell method, comparing it with a low order finite element computation and using the *same* framework software [6]. Since the FCM inherits the fast convergence property of the p-extension, the CPU time is much shorter than of the linear h-extension. For the current example, a finite element approximation with 57,212 linear elements result in an error of 0.8% in the energy norm, in 106 s. A finite cell solution with only four cells ($p = 8$, integration subcells: 10×10, Gaussian points: 10 in each direction) results in an error of 0.43% in only 7 s. One may notice, moreover, that the finite cell method saves also the time required for meshing and pre-processing, which is not relevant for the given example but which can be considerable for complex domains.

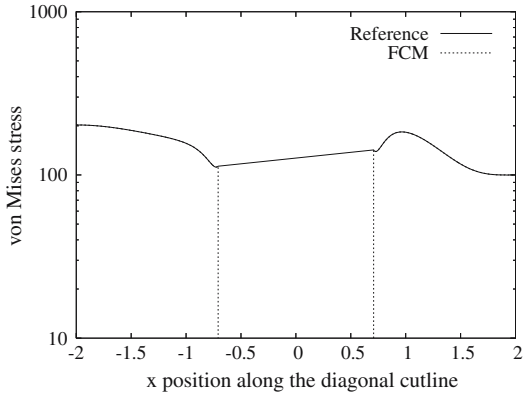

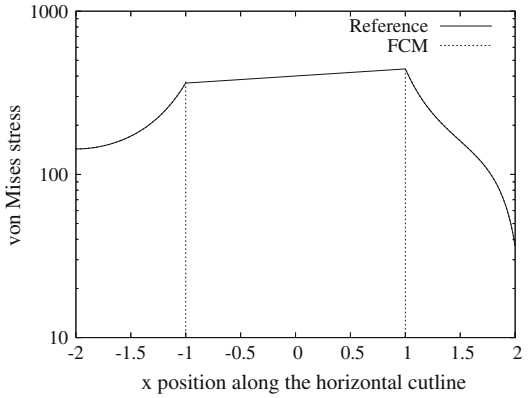

Fig. 8 von Mises stress for the symmetric perforated plate: Reference solution and FCM approximation along the diagonal cut-line from $(-2, -2)$ to (2,2) and horizontal cut-line from $(-2, 0)$ to (2,0), top and bottom, respectively

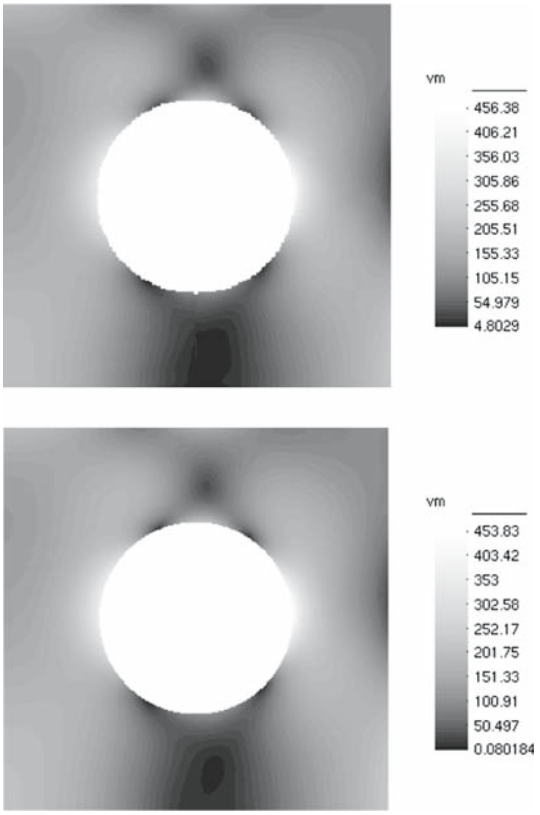

Fig. 9 Contours of von Mises stress for the perforated plate, FCM (*top*) with four cells, $p = 10$, and reference solution (*bottom*)

3.1.3 Dirichlet boundary conditions

Let us now consider the perforated plate again, but with boundary conditions as shown in Fig. 10 (top). An $\alpha = O(10)$ is used to take into account the essential boundary condition on the lower boundary in an extended domain (bottom). In contrast to earlier examples with structured cells, now a mesh of 26 unstructured cells is used which do not conform to the essential boundary, but only to the corners $(-2, -2)$ and $(2, -2)$ of the domain Ω. To avoid rigid body motion the lower boundary of the extended domain is fixed. The reference strain energy is 0.7511036269, and the strain energy achieved by the current model is 0.7510342384 for $p = 11$ yielding an error in the energy norm of 0.96%. Figure 10 shows the von Mises stress contours in the domain Ω. Figure 11 compares the von Mises stress along the cut-lines $[(-2, -2), (2, 2)]$ and $[(-2, 0), (2, 0)]$. As shown, the stresses along these cut-lines enjoy an excellent accuracy.

It is important to note that the strain energy as given above is computed only for the physical domain Ω of the perforated plate, while the artificial support, as shown in Fig. 10, is not completely rigid and behaves like an elastic support being α times stiffer than the main material of the actual structure.

If cell nodes do not match domain corners at all, we will have cells which incorporate three different αs. In the material part, $\alpha = 1$, in the void part $\alpha << 1$ and in the rigid part $\alpha >> 1$. This introduces a (mild) singularity interior to a cell (Case 3 as discussed in Sect. 2.4). Figure 12 shows an unstructured cell mesh which is used for the perforated plate; 58 cells are used and the strain energy is 0.7503773736 for $p = 12$. The diagonal cut-line shows a significant deviation only in the corner cell.

3.2 Porous domain

In this example the method is investigated for problems with many inclusions. The meshes for the reference finite element solution and for FCM are shown in Fig. 13, where a plate under tension is perforated with 49 holes. The lower boundary is clamped and other boundary conditions and mechanical properties are as given before and in Fig. 4. Holes, $(r = 0.1)$, are distributed equidistantly with a step of 0.5 in each direction. A mesh of 41×41 square cells is used with $p = 8$. Sub-cells to perform accurate integration are not

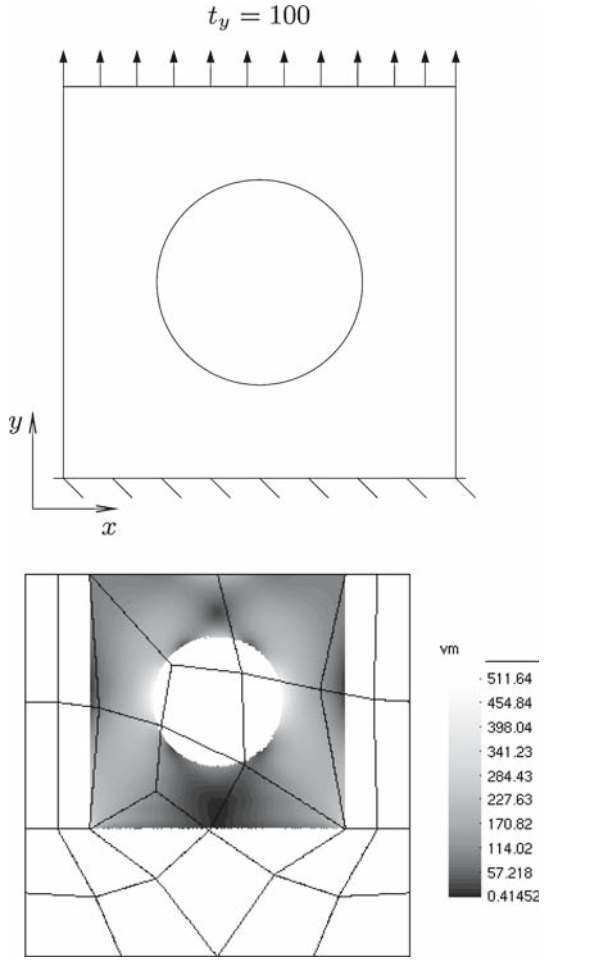

Fig. 10 The perforated plate $[(-2,-2),(2,2)]$ (*top*) is embedded in an extended domain $[(-3,-4),(3,2)]$ covering the Dirichlet boundary. von Mises contours are given for the domain Ω, only (*bottom*)

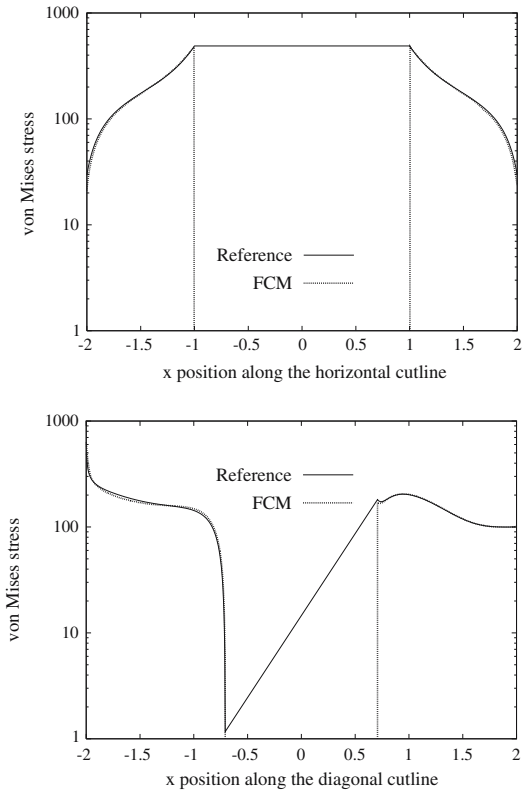

Fig. 11 von Mises stress along the horizontal (*top*) and diagonal (*bottom*) cut-lines for the perforated plate embedded in an extended domain while cells match the singular corners

necessary. The reference solution is obtained by a fine quasi-uniform unstructured mesh of 6,106 elements while p is increased to 8 to ensure convergence. Figure 14 gives the stress contours and Fig. 15 compares the stress distribution along the diagonal cut-line, which is in very good agreement with the reference solution while the maximum error is less than 1%.

3.3 Singularities due to reentrant corners

The capacity of the method when strong singularities exist in the domain will now be investigated. In this example the circular hole of Fig. 4 is replaced by a square inclusion, yielding four reentrant corners to the domain of computation. A reference solution is obtained from a p-extension on a geometrically refined mesh and yields a strain energy of 0.8618383790 with 66,334 DOF ($p = 16$).

3.3.1 Cells do not conform to singularities

If the cells happen to conform to the edges and singular corners, the rate of convergence for FCM would be the same as the rate of a uniform finite element p-extension [23,24]. Let us instead continue with 11×11 cells that do *not* match any singular corner or edges of the problem. Figure 16 shows (top) this discretized domain and the convergence history of the energy norm using a FCM-p-extension to an error of about 4% (bottom). The convergence rate is now, as stated in Sect. 2.4 slower than for a FEM-h-extension.

To show the accuracy of pointwise stress values let us consider a critical cut-line passing through the singular points of the square corners from $(-2,-2)$ to $(2,2)$. The stress distribution along this cut-line is given in Fig. 17 for $p = 8$ and an integration with 4×4 sub-cells in the cut cells. This figure suggests that the only region of the problem that contributes significantly to the error in strain energy, thus to the slow convergence observed in Fig. 16, is in the very close vicinity of the singular point. However the finite cell method reveals well the singular nature of the problem although the cells do not match the singular points or edges at all.

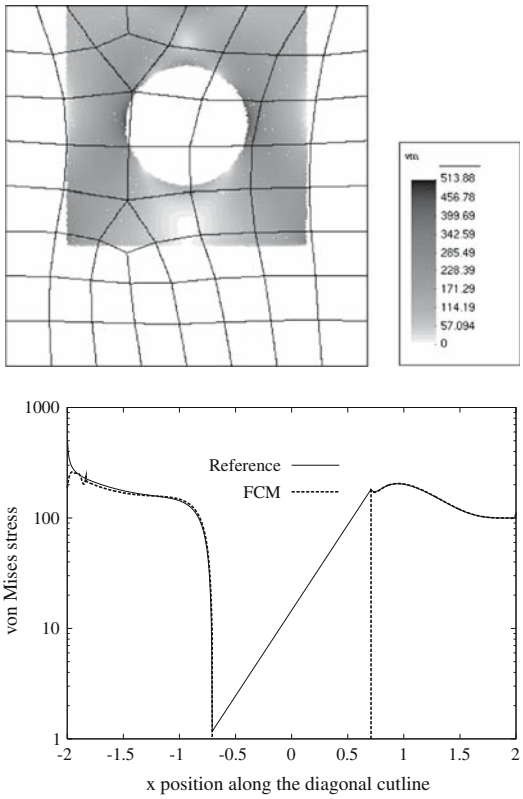

Fig. 12 von Mises stress contours for the perforated plate embedded in an unstructured cell (*top*), and along the diagonal cut-line (*bottom*)

3.3.2 Cells conform to singularities

To improve the convergence rate, we switch to an arrangement of unstructured cells that only conform to the singular corners but not to the edges of the rectangular inclusion. This unstructured mesh with 30 cells is shown in Fig. 18 and the convergence curve for a p-extension is again given in Fig. 16. The convergence rate is about twice that of a FEM-h-version ($p = 1$) on a quasi-uniform, unstructured mesh.

3.3.3 Singularities replaced by fillets

To further investigate properties of the finite cell method, the sharp singular corners are replaced by filleted corners. Figure 19 shows the mesh of 11×11 cells taken while 4×4 sub-cells are used to integrate over the cells cut by the boundary. As shown, neither edges nor corners of the square conform to the cells. Each sharp corner is replaced by a fillet of radius r. Figure 20 gives the convergence history of the energy norm while the reference strain energies are 0.8598533837, 0.856372672, 0.850013301, 0.8361299289, respectively for $r = 0.02, 0.05, 0.1$ and 0.2. Since the cell size is $\frac{4}{11}$, one may conclude that for fillet radii bigger than $0.275(= 0.1/(\frac{4}{11}))$ of the cell size, preasymtotic exponential

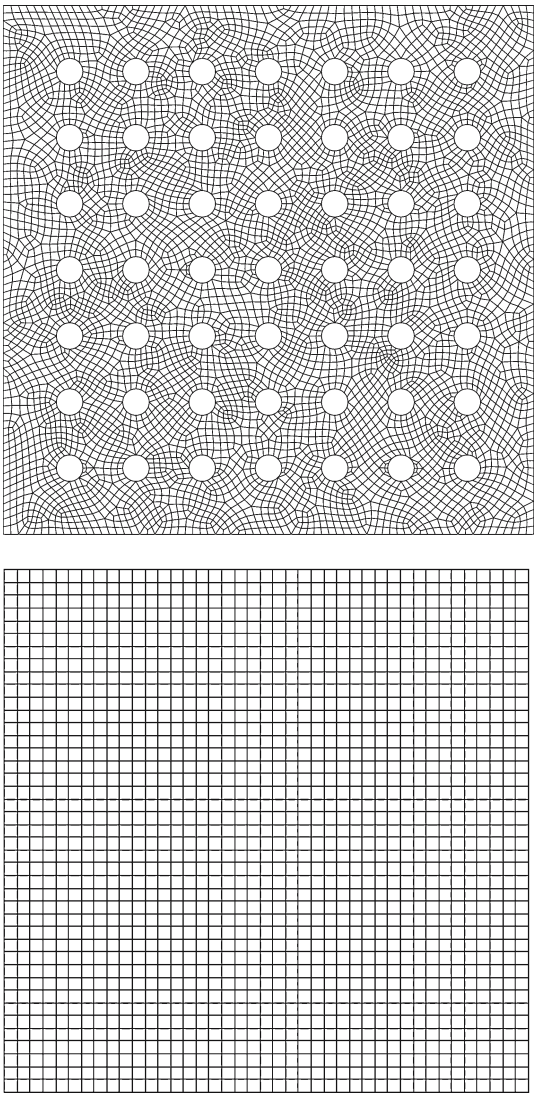

Fig. 13 Porous problem. The model used for the reference solution has 6,106 quadrilateral elements (*top*) while the FCM model has 41×41 cells (*bottom*)

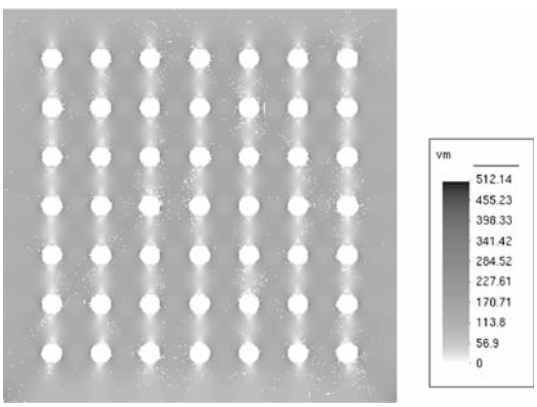

Fig. 14 Porous problem. von Mises stress contours by FCM

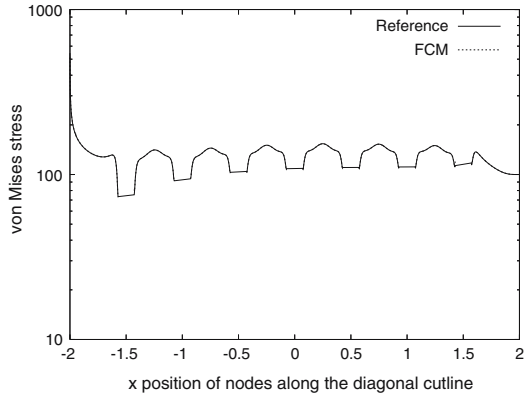

Fig. 15 Porous domain. von Mises stress distribution by FCM and the reference solution along the diagonal cut-line from $(-2, -2)$ to (2,2). Since the results enjoy almost perfect agreement, it is difficult to differentiate between them at this scale

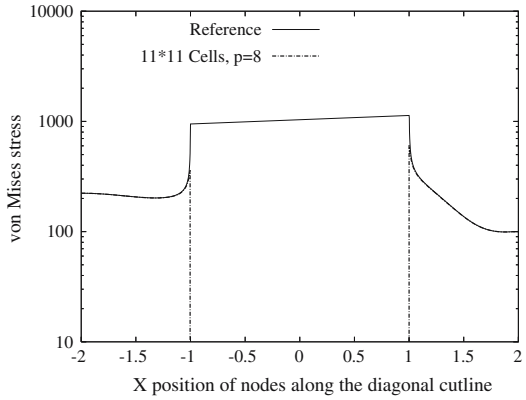

Fig. 17 Singular problem. von Mises stress distribution by FCM and the reference solution along the diagonal cut-line from $(-2, -2)$ to (2,2)

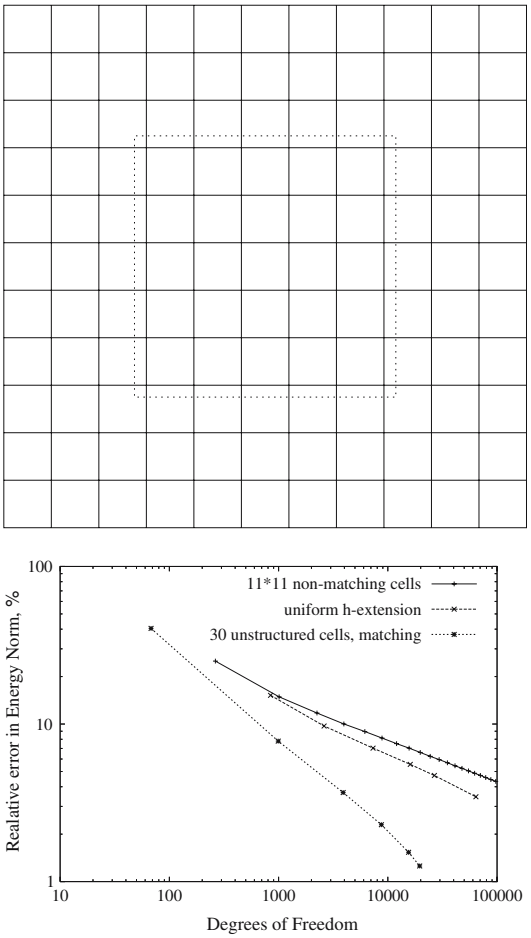

Fig. 16 The singular perforated plate is discretized using 11×11 cells (*top*). The error in the energy norm versus DOF (*bottom*)

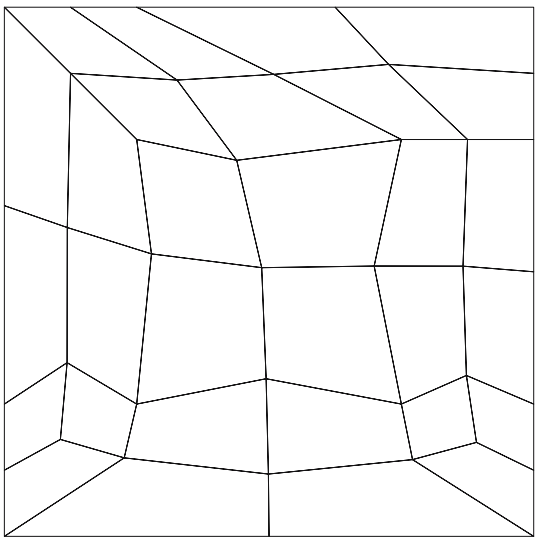

Fig. 18 A simple unstructured cell matching only the singular corners of the internal inclusion

3.3.4 Macro cells for singularities

In another attempt, we examined a macro cell pattern enclosing the singular points without necessarily conforming to them, Fig. 21. This macro is applied to produce a mesh of 57 cells, Fig. 22. The convergence history for two different number of integration sub-cells is given in Fig. 23. As shown, exponential preasymptotic convergence is achievable even though the nodes and singular corners do not conform.

4 Conclusions

convergence rate and high accuracy of the solution can be observed.

The finite cell method, as described in this paper, is based on a simple concept which can be implemented with little

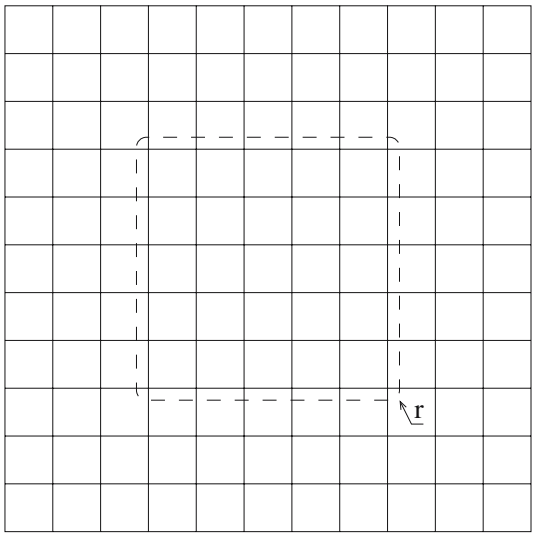

Fig. 19 A mesh of 11 × 11 cells is used and the sharp corners are replaced by filleted corners of radius *r*

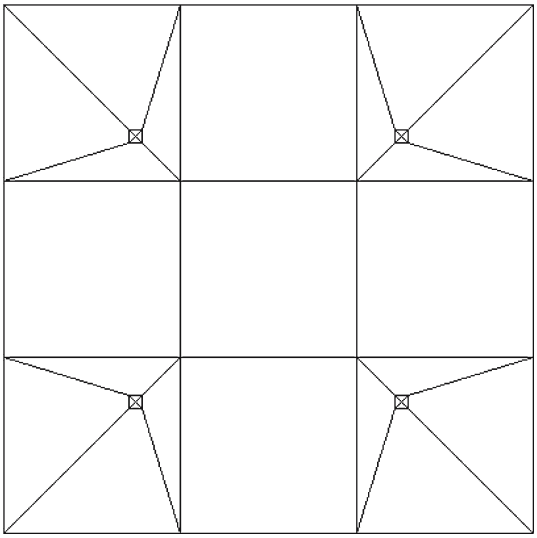

Fig. 22 The macro is used to create a mesh of 57 cells for the singular problem

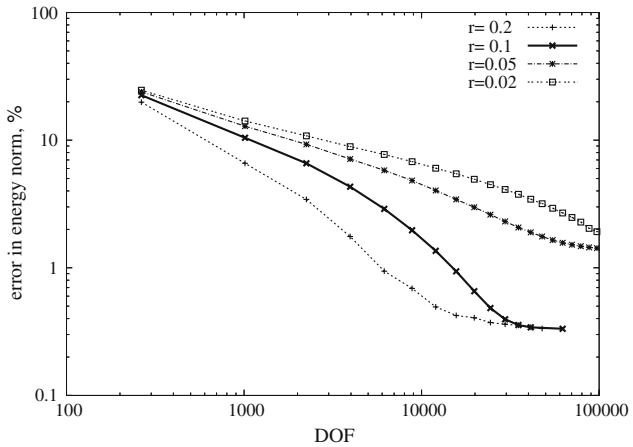

Fig. 20 The convergence history for various radii

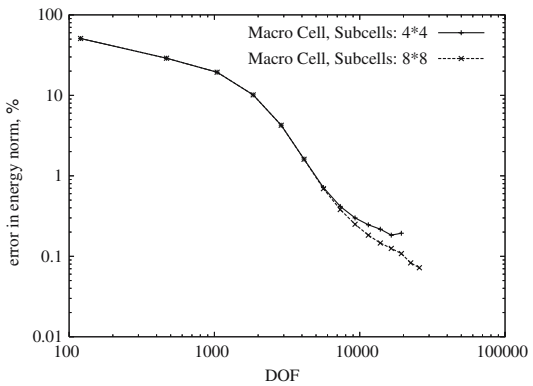

Fig. 23 Preasymptotic exponential convergence rate for different numbers of integration sub-cells

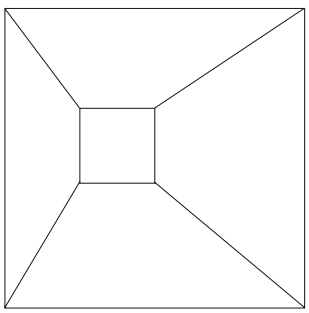

Fig. 21 A macro is defined to refine the cells around singularities

effort, during the integration process, if a *p*- or *h*-version finite element code is available. The convergence rate for regular problems using an *h*-extension is the same as for the *h*-version FEM, while exponential convergence is achievable using *p*-extension. For singular problems algebraic rate of convergence is attainable which can be improved if the singular points are met by cell nodes or if special macro cell patterns are used.

The integration of stiffness matrices and load vectors is performed on an embedding domain. The performance of the method can certainly be increased if suitable adaptive integration algorithms, such as quadtree based schemes, are taken for the critical cut cells. Further research can be carried out to apply the idea to problems with moving boundaries and porous materials. Although the algorithm has been only investigated for 2D elasticity problems in this paper, it is applicable to other differential equations and 3D-problems as well. Results will be reported in a forthcoming paper [7].

References

1. Allaire G, Jouve F, Toader A (2004) Structural optimization using sensitivity analysis and a level-set method. J Comp Phys 194/1:363–393
2. Badea L, Daripa P (2001) On a boundary control approach to domain embedding methods. SIAM J Control Optim 40(2):421–449
3. Chen Y, Lee J, Eskandarian A (2006) Meshless methods in solid mechanics. Springer, Heidelberg
4. Del Pino S, Pironneau O (2003) A fictitious domain based general PDE solver. In: Kuznetsov Y, Neittanmaki P, Pironneau O (ed) Numerical methods for scientific computing variational problems and applications. CIMNE, Barcelona
5. Duarte CAM, Babuška I, Oden JT (2000) Generalized finite element method for three-dimensional structural mechanics problems. Comput Struct 77(2):215–232
6. Düster A, Bröker H, Heidkamp H, Heißerer U, Kollmannsberger S, Krause R, Muthler A, Niggl A, Nübel V, Rücker M, Scholz D, AdhoC^4-user's guide, Lehrstuhl für Bauinformatik, Technische Universität München
7. Düster A, Parvizian J, Yang Z, Rank A (2007) The finite cell method for 3D problems of solid mechanics, under preparation
8. http://www.gid.cimne.upc.es
9. Glowinski R, Pan T-W, Hesla TI, Joseph DD (1999) A distributed lagrange multiplier/fictitious domain method for particulate fows. Int J Multiph Flow 25:755–794
10. Ismail M (2004) The fat boundary method for the numerical resolution of elliptic problems in perforated domains. Application to 3D Fluid Flows. PhD thesis, University Pierre and Marie Curie-Paris VI, France
11. Neittaanmäki, Tiba D (1995) An embedding domains approach in free boundary problems and optimal design. SIAM Control Optim 33(5):1587–1602
12. Osher S, Fedkiw R, Level-Set Methods and Dynamic Implicit Surfaces. Springer, Heidelberg
13. Paffrath M, Jacobs W, Klein W, Rank E, Steger K, Weinert U, Wever U (1993) Concepts and algorithms in process simulation. Surv Math Ind 3, S.149–183
14. Ramiére I (2006) Méthodes de domaine fictif pour des problèmes elliptiques avec conditions aux limites générales en vue de la simulation numrique d'écoulements diphasiques. PhD Thesis, UNIVERSITÉ DE PROVENCE - AIX-MARSEILLE I, France
15. Ramiére I, Angot P, Belliard M (2007) A fictitious domain approach with spread interface for elliptic problems with general boundary conditions. Comput Methods Appl Mech Eng 196(4–6):766–781
16. Rank E, Werner H (1986) An adaptive finite element approach for the free surface seepage problem. Int J Numer Methods Eng 23:1217–1228
17. Rank E (1989) Local oxidation of silicon—a finite element approach. In: Bank RE, Bulirsch R, Merten K (eds) Mathematical modelling and simulation of electrical circuits. Birkhuser Verlag, Berlin
18. Rank E (1991) Finite-element-simulation of local oxidation in semiconductor processing, In: Whitemann JR (ed) The mathematics of finite elements and applications VII. Academic, New York
19. Rusten T, Vassilevski PS, Winther R (1998) Domain embedding preconditioners for mixed systems. Numer Linear Algebra Appl 5:321–345
20. Sethian JA (1999) Level-Set Methods and Fast Marching Methods. Cambridge University Press, Cambridge
21. Singh KM, Williams JJR (2005) A parallel fictitious domain multigrid preconditioner for the solution of Poisson's equation in complex geometries. Comput Methods Appl Mech Eng 194:4845–4860
22. Strouboulis T, Babuška I, Copps K (2000) The design and analysis of the generalized finite element method. Comput Methods Appl Mech Eng 181:43–69
23. Szabó BA, Düster A, Rank E (2004) The *p*-version of the finite element method. In: Stein E, de Borst R, Hughes TJR (eds) Encyclopedia of computational mechanics, Vol. 1, Chapter 5. Wiley, New York, pp. 119–139
24. Szabó BA, Babuška I (1991) Finite element analysis. Wiley, New York
25. Zhou YC, Wei GW (2006) On the fictitious-domain and interpolation formulations of the matched interface and boundary (MIB) method. J Comp Phys 219:228–246